

1 **THE REACTION MECHANISM OF METALLO- β -LACTAMASES IS**
2 **TUNED BY THE CONFORMATION OF AN ACTIVE SITE MOBILE LOOP**

3
4 **Antonela R. Palacios^{1*}, María F. Mojica^{2,3*†}, Estefanía Giannini¹, Magdalena A.**
5 **Taracila^{3,4}, Christopher R. Bethel³, Pedro M. Alzari⁵, Lisandro H. Otero^{6,7}, Sebastián**
6 **Klinke^{6,7}, Leticia I. Llarrull^{1,8}, Robert A. Bonomo^{2,3,4,9,10,11} and Alejandro J. Vila^{1,7, 8,11}**

7
8 **Running title:** Mobile loop tunes reaction mechanism of M β Ls

9
10 ¹ Instituto de Biología Molecular y Celular de Rosario (IBR, CONICET-UNR), Ocampo y
11 Esmeralda, S2002LRK Rosario, Argentina;

12 ² Department of Biochemistry, Case Western Reserve University School of Medicine,
13 Cleveland, Ohio, USA;

14 ³ Research Service, Louis Stokes Veterans Affairs Medical Center, Cleveland, Ohio, USA;

15 ⁴ Department of Medicine, Case Western Reserve University School of Medicine,
16 Cleveland, Ohio, USA;

17 ⁵ Institut Pasteur, Unite de Microbiologie Structurale, CNRS UMR 3528 & Université Paris
18 Diderot, 25 rue du Docteur Roux, 75724 Paris, France;

19 ⁶ Fundación Instituto Leloir, IIBBA-CONICET, Buenos Aires, Argentina;

20 ⁷ Plataforma Argentina de Biología Estructural y Metabólica PLABEM, Buenos Aires,
21 Argentina;

Mobile loop tunes reaction mechanism of metallo- β -lactamases

22 ⁸ Área Biofísica, Facultad de Ciencias Bioquímicas y Farmacéuticas, Universidad Nacional
23 de Rosario, S2002LRK Rosario, Argentina;

24 ⁹ Departments of Medicine, Pharmacology, Molecular Biology and Microbiology,
25 Biochemistry, Proteomics and Bioinformatics, Case Western Reserve University School of
26 Medicine, Cleveland, Ohio, USA;

27 ¹⁰ Medical Service and GRECC, Louis Stokes Cleveland Department of Veterans Affairs
28 Medical Center, Cleveland, Ohio, USA;

29 ¹¹ CWRU-Cleveland VAMC Center for Antimicrobial Resistance and Epidemiology (Case
30 VA CARES), Cleveland, Ohio, USA.

31 * These authors contributed equally to this work.

32 ≠ Present address: Grupo de investigación en Resistencia Antimicrobiana y Epidemiología
33 Hospitalaria – RAEH. Universidad El Bosque. Av 9 No. 131 – 02. Bogotá, Colombia.

34

35 Address correspondence to Alejandro J. Vila vila@ibr-conicet.gov.ar and Robert A Bonomo
36 rab14@case.edu

37

38 **ABSTRACT**

39 Carbapenems are “last resort” β -lactam antibiotics, used to treat serious and life-
40 threatening healthcare-associated infections caused by multidrug resistant Gram-negative
41 bacteria. Unfortunately, the worldwide spread of genes coding for carbapenemases among
42 these bacteria is threatening these life-saving drugs. Metallo- β -Lactamases (M β Ls) are the
43 largest family of carbapenemases. These are Zn(II)-dependent hydrolases that are active
44 against almost all β -lactam antibiotics. Their catalytic mechanism and the features driving
45 substrate specificity have been matter of intense debate. The active sites of M β Ls are
46 flanked by two loops, one of which, loop L3, was shown to adopt different conformations
47 upon substrate or inhibitor binding, and thus being expected to play a role in substrate
48 recognition. However, the sequence heterogeneity observed in this loop in different M β Ls
49 has limited the generalizations about its role. Herein we report the engineering of different
50 loops within the scaffold of the clinically relevant carbapenemase NDM-1. We find that the
51 loop sequence dictates its conformation in the unbound form of the enzyme, eliciting
52 different degrees of active site exposure. However, these structural changes have a minor
53 impact on the substrate profile. Instead, we report that the loop conformation determines
54 the protonation rate of key reaction intermediates accumulated during the hydrolysis of
55 different β -lactams in all M β Ls. This study demonstrates the existence of a direct link
56 between the conformation of this loop and the mechanistic features of the enzyme, bringing
57 to light an unexplored function of active site loops on M β Ls.

58

59

60 INTRODUCTION

61 β -Lactams are the most frequently prescribed class of clinically available antibiotics,
62 used to treat infections caused by both Gram-negative and Gram-positive bacteria. β -
63 Lactams inhibit bacterial cell wall synthesis by targeting transpeptidases and
64 carboxypeptidases (bacterial cell wall synthesizing enzymes) (1). The main mechanism of
65 bacterial resistance against β -lactams in Gram-negative bacteria is the expression of β -
66 lactamases, enzymes that selectively hydrolyze the β -lactam ring, rendering the antibiotic
67 ineffective (2, 3). Two distinct types of β -lactamases are currently known: serine- β -
68 Lactamases, which employ a Ser residue as the active nucleophile in catalysis, and
69 metallo- β -Lactamases (M β LS), which are metal-dependent hydrolytic enzymes. M β LS are of
70 medical concern given their ability to hydrolyze and confer resistance to virtually all classes
71 of β -lactam antibiotics. Notably, all M β LS show hydrolytic capacities against carbapenems,
72 the most potent β -lactam antibiotics to date, routinely used as "last resort drugs" (1).
73 Although some compounds have been found to be effective as M β L inhibitors (4-12), none
74 of them are available to treat clinical infections yet, giving rise to a crisis in antimicrobial
75 chemotherapy (13-18).

76 M β LS are subdivided in 3 subclasses (B1, B2 and B3) based on the identity of active site
77 essential residues, Zn(II) requirements and substrate profile (15, 16, 19-22). B1 M β LS are
78 those of major clinical concern, because they are broad substrate spectrum β -lactamases
79 and are encoded on mobile genetic elements in pathogenic and opportunistic bacteria. The
80 most clinically relevant B1 lactamases belong to the NDM (New Delhi Metallo- β -
81 Lactamase), VIM (Verona Integron-encoded M β L), and IMP (Imipenemase M β L) families,
82 with NDM-1, VIM-2 and IMP-1 being the most widespread allelic variants. In particular,
83 NDM-1 is a membrane-anchored enzyme (23) and is one of the most widespread M β LS

84 with a potent carbapenemase activity (16, 24, 25).

85 Two Zn(II) ions are required for the catalytic activity of B1 M β Ls (26, 27). Both Zn(II)
86 atoms are bound to a conserved ligand set: one Zn(II) ion is coordinated to three His
87 residues (116, 118 and 196, after the standard BBL numbering (28)) and a hydroxide
88 molecule (3H site), whereas the other is bound to the same (bridging) OH, an extra water
89 molecule and residues Asp120, Cys221 and His263 (DCH site) (29-31). The metal ion at
90 the DCH site has been shown to be essential in stabilizing key reaction intermediates
91 during hydrolysis of chromogenic cephalosporins (32) and carbapenems (33, 34). This
92 active site is located in a shallow and broad groove flanked by two loops: active site loop
93 L10, and active site loop L3. Amino acid substitutions in both loops are associated with
94 changes in the substrate profile in B1 M β Ls (35-40). Despite different families of B1 M β Ls
95 present a conserved active site and global protein fold, these β -lactamases share very low
96 sequence identity. This diversity has posed additional challenges for the development of an
97 M β L inhibitor. Thus, the identification of common and distinct features is crucial for the
98 understanding of their mechanism and substrate recognition profile.

99 Loop L3 has been the focus of several studies in M β Ls. Crystallographic and NMR
100 studies identified variable conformations of this loop in many B1 M β Ls (38, 41-45), and its
101 role in specific interactions with their substrates is well documented (36, 39, 44, 46).
102 Moreover, an increase of the dynamics of this loop was hypothesized with the broadening
103 of the substrate profile in an *in vitro* evolved lactamase (37). The consensus identifies loop
104 L3 as a mobile flap able to adapt its conformation upon small molecule binding in the active
105 site. However, the sequence heterogeneity observed in the loop L3 from different M β Ls has
106 limited generalizations about its specific role.

107 To explore the role of the loop L3 in the scaffold of NDM-1, we designed a series of

108 variants in which we replaced the native loop by those of IMP-1 or VIM-2, and a third one in
109 which a Pro residue was introduced at the C-terminus of the loop. Herein we show that the
110 substrate spectra and the active site structure display minor perturbations in these chimeric
111 proteins, despite previous expectations. Crystal structures of two of the obtained chimeras
112 show that different loops in the same scaffold adopt quite different conformations, spanning
113 from an open to a close active site in the unbound form of the enzyme. However, the loop
114 conformation cannot correlate to the substrate profile observed for the different variants.
115 Instead, the loop conformation directly impacts on the accumulation of the anionic reaction
116 intermediates, disclosing an auxiliary structural determinant of the mechanism of hydrolysis.
117 These findings suggest a new role of this mobile loop in the catalytic mechanism of M β Ls.

118

119 **RESULTS**

120 **Loop L3 engineering gives rise to active and stable NDM variants**

121 A closer look at the primary sequence of the loop L3 of IMP-1, VIM-2 and NDM-1
122 reveals significant differences (Fig. 1). For instance, the loop L3 of IMP-1 displays the same
123 length as that from NDM-1, but it contains more polar residues. In contrast, the VIM-2 loop
124 L3 shows a similar charge distribution but is one residue shorter and less hydrophobic than
125 NDM-1 loop L3. Also, a proline residue is located at the C-terminus of the loop in all cases,
126 except in NDM-1. To study the function of loop L3 in NDM-1, we designed two chimeric
127 proteins in which the NDM-1 loop was replaced by the loops of IMP-1 and VIM-2 (including
128 the Pro residues). These variants were designated as L3IMP and L3VIM, respectively. In
129 order to assess how an insertion could impact in the function of loop L3, we also
130 engineered an extra M β L in which a Pro residue was inserted at the base of the NDM-1
131 loop, the L3Pro variant.

132 We used both *in bacteria* and *in vitro* approaches to analyze the L3 variants.
133 *Escherichia coli* cells expressing the chimeric proteins were used to analyze M β Ls
134 properties in a natural background. We evaluated the expression levels in whole cells,
135 spheroplasts and periplasmic extracts by immunoblotting (Fig. 2A). All variants were
136 expressed including the native leader peptide of NDM-1, containing the canonical lipitation
137 sequence LSGC (lipobox), which anchors the protein to the inner leaflet of the outer
138 membrane (23, 43). None of the variants was in the periplasmic extracts, revealing an
139 adequate processing of the leader peptide. The analysis of whole cell extracts and
140 spheroplasts showed that NDM-1 and variants L3IMP and L3Pro showed similar expression
141 levels and that the L3VIM variant was expressed at lower levels, but without compromising
142 protein stability (Fig. 2A). These experiments show that our loop L3 engineering has been
143 successful in eliciting stable proteins.

144 We next tested the susceptibility of *E. coli* cells expressing the three NDM-1 L3 variants
145 against a broad panel of β -lactam antibiotics. Minimal inhibitory concentration (MIC)
146 analyses (Table 1) reveal that the L3 variants confer somehow lower levels of resistance
147 against all tested substrates. In the case of cefepime, the impact of the mutations in the
148 MIC values is larger. M β Ls with reduced Zn(II) binding capabilities provide lower levels of
149 resistance because metal binding takes place in the periplasmic space where Zn(II)
150 availability is limited (26, 47, 48). We tested the effect of Zn(II) deprivation on protein
151 expression levels by treating *E. coli* cells expressing NDM-1 variants with the metal chelator
152 dipicolinic acid (DPA). This chelator strongly affected the expression of L3Pro and L3VIM
153 variants, while the impact was moderate for variant L3IMP and wild type NDM-1 (Fig. 2B).
154 We also tested the ability of our NDM-1 variants to bind Zn(II) within the cell by determining
155 the impact of DPA in the MIC values against cefotaxime. The sensitivity of L3IMP to Zn(II)

156 deprivation resembled that of NDM-1, whereas it was increased for L3Pro and even more
157 for the L3VIM variant (Fig. 2C).

158 We then expressed and purified all variants in the soluble form, a truncated version in
159 which the first 38 residues, including the signal peptide and the lipidation site, were
160 removed (Δ 38). All variants were obtained by expression in rich (LB) medium with similar
161 yields as the wild type NDM-1, except for L3VIM, for which yields one order of magnitude
162 lower were obtained. Also, the Zn(II) affinity of L3VIM was lower than the other variants
163 (Table S1). This could explain the higher sensitivity of L3VIM when challenged with DPA
164 (Fig. 2C) and the lower metal content (Materials and Methods section).

165 We measured the stability of the purified variants and their apo-derivatives by thermal
166 shift analysis (Table 2). The L3 variants were slightly less stable than the wild type enzyme,
167 with T_M values spanning a narrow range (4 °C). Instead, the non-metallated forms displayed
168 a more pronounced destabilization effect. The L3VIM variant features the largest gap
169 between the T_{MS} of metallated and non-metallated forms, indicating that in this case the
170 Zn(II) ions play a crucial role in stabilizing the M β LS. These results added to the differences
171 on the expression levels under DPA addition, demonstrate that the stability of the non-
172 metallated form determines steady state protein expression levels and confirms that the
173 metal uptake in the periplasm is crucial for M β LS stability.

174 The activity of the enzymes was then studied by steady-state kinetics using purified
175 M β LS. The determined k_{cat}/K_M values were within the same range of those measured for
176 NDM-1 and all variants showed broad substrate spectra (Table 3). In general, the L3Pro
177 variant displayed the lowest catalytic efficiencies, and L3IMP was the only variant that was
178 catalytically more efficient compared to NDM-1 against some penicillins and
179 cephalosporins. We stress that L3Pro displayed both elevated K_M and k_{cat} values, with

180 larger increases in K_M resulting in overall lower catalytic performances. The kinetic
181 parameters measured for L3VIM, in contrast, are closer to those of NDM-1. As L3VIM
182 present a lower expression level than NDM-1 (Fig. 2A), it is likely that the MICs values
183 obtained may have been lower due to a decreased expression level or Zn(II) uptake in the
184 periplasm. The hydrolysis parameters for nitrocefin were practically unaltered upon loop
185 replacement. On the other hand, for carbapenem hydrolysis both K_M and k_{cat} values
186 presented differences within the variants: L3IMP parameters were lower than the wild type
187 values, and for L3VIM and L3Pro these values were higher than in the wild type enzyme.
188 Notwithstanding these changes in the substrate preferences, a clear trend in the substrate
189 profile elicited by the loop replacement could not be identified in the chimeric proteins.

190 **Loop L3 conformation models the active site cavity size and accessibility with minor** 191 **alterations on metal ligands**

192 Although residues in loop L3 do not directly interact with the Zn(II) ions, the different
193 sensitivities to Zn(II) deprivation prompted us to test whether the loop L3 replacements
194 induced changes in the metal binding sites in the variants. For that purpose, we used Co(II)
195 as a spectroscopic probe of the metal site coordination geometry, replacing the
196 spectroscopically silent Zn(II) ion (49). Fig. 3 shows the electronic absorption difference
197 spectra in the UV-Vis range of all Co(II) derivatives. These spectra are characterized by
198 distinctive features in two regions: (1) the Laporte-forbidden $d-d$ transitions in the visible
199 range (450–650 nm), which provide information on the metal site geometry (mainly of the
200 3H site); and (2) a ligand-to-metal charge transfer transition (LMCT), ca. 330 nm, which
201 reports on the Cys-Co(II) interaction at the DCH site (29). The band pattern and intensity of
202 the $d-d$ bands were preserved in all variants, revealing that the geometry at the 3H site was
203 conserved (Fig. 3). The Co(II) derivatives displayed subtle changes on the position and

204 intensity of the LMCT band, which reflects minor changes in the Co(II)-thiolate interactions
205 at the DCH site, especially for the L3Pro and L3VIM variants. These results suggest that
206 loop replacement did not significantly alter the coordination sphere of the metal ion in the
207 active site.

208 To rationalize the impact of changes in loop L3, we performed X-ray crystallographic
209 studies. The L3IMP and L3Pro variants were crystallized, and both structures were solved
210 at a resolution of 1.65 and 1.80 Å, respectively (Table S2). Attempts to obtain crystals of the
211 L3VIM variant were unsuccessful. The structures of both variants are very similar to the
212 previously reported crystal structure of native NDM-1 (PDB code: 3SPU) (43). The overall
213 structure of the enzymes and their active sites are highly conserved (Fig. 4A), as accounted
214 for the low rmsd values of the core structure without considering the loop L3 (< 0.60 Å over
215 all Ca). The active sites of L3IMP and L3Pro displayed bimetallic occupancy, *i.e.*, with metal
216 ions at the 3H and the DCH sites. The presence of Zn(II) was verified by anomalous
217 diffraction. In the case of L3Pro, peaks of 40-50 rmsd were observed at the 3H site,
218 confirming the presence of Zn(II), while no signal was observed at the DCH site (Fig. S1).
219 Instead, the electron density could be properly accounted for by assuming the presence of
220 Cd(II) (from the crystallization buffer) at this position. This metal substitution with a
221 preserved geometry at the active site has already been reported for NDM-1 (3ZR9) (41).

222 The structures did not reveal significant changes in the metal binding sites (Fig. 4B).
223 The position of the Zn(II) ion and the three ligands in the 3H site remains unaltered among
224 the L3 variants. In the DCH site, despite the different identity of the metals (Zn(II) in L3IMP
225 and Cd(II) in L3Pro), a variation of only 0.5 Å for the metal ion position was observed, with
226 the ligand residues displaying identical conformations. This observation agrees with the

227 spectroscopic data on the Co(II)-substituted enzymes that reveal a slightly perturbed DCH
228 site, and a conserved geometry at the 3H site.

229 The conformation of loop L3, instead, is considerably different among the variants (Fig.
230 4C). The electron density is well defined in these loops in both variants, with B-factors
231 slightly higher than those in the protein core (around 20 and 30 Å² higher for L3IMP and
232 L3Pro, respectively) (Fig. S2). In L3Pro, the interactions among the residues shaping the β -
233 sheet at the base of loop L3 are disrupted by the insertion of a Pro residue, giving rise to a
234 more open loop conformation. In the case of L3IMP, the loop is stabilized by hydrophobic
235 interactions of Trp64 with residues His263, Val67 and Val61, which pull Trp64 towards the
236 active site inducing a more closed conformation of the loop (Fig. S3). The angle subtended
237 by Zn1, the C α atom of Ser69 (located on the base of loop L3) and the C α atom of Gly63
238 (located on the tip of the loop), provides a *bona fide* description of the loop 3 conformation
239 (the larger the angle, the more open the loop), varying from 68° (L3IMP), 88° (NDM-1) to
240 110° (L3Pro) (Fig. 4C). Thus, the L3 sequence dictates the conformation of the loop in the
241 unbound form of this enzyme within the same protein scaffold.

242 **Loop L3 determines the accumulation of catalytic reaction intermediates**

243 The catalytic mechanism of M β LS takes place by accumulation of an anionic
244 intermediate that has been characterized for the hydrolysis of the chromogenic
245 cephalosporin, nitrocefin, and several carbapenems (33, 34, 50, 51). The rate-determining
246 step of the reaction is, in both cases, the protonation of this intermediate, leading to the final
247 product. Moali *et al.* reported that changes in loop L3 altered the accumulation of the
248 intermediate during nitrocefin hydrolysis (39). Thus, we decided to study the hydrolysis of
249 nitrocefin and carbapenems by our variant M β LS under pre-steady-state conditions with a
250 photodiode array (PDA) detector coupled to a stopped-flow mixing device (32, 33).

251 Three absorption bands are observed during nitrocefin hydrolysis at 390, 485 and
252 605 nm, which correspond to the substrate, product, and the anionic intermediate of the
253 reaction, respectively (Fig. 5A) (32, 50). When we performed the hydrolysis reaction with all
254 the L3 variants, the three bands were evidenced with similar maximum absorbance
255 intensities (Fig. 5B). An analysis of the time course of the reaction (Fig. 5C) reveals that the
256 time frame for accumulation and decay of the intermediate is similar for NDM-1 and the
257 L3IMP variant, with L3IMP displaying the intermediate with the longest accumulation time.
258 Instead, the intermediate is less stable in the L3VIM and, specially, L3Pro variants.
259 Supporting this line, product formation is evidently faster in L3Pro, followed by L3VIM,
260 NDM-1 and L3IMP; indicating that the decrease on the accumulation of the reaction
261 intermediate is due to an increment on the protonation rate. Substrate consumption is also
262 slower in NDM-1, and L3IMP, which could also contribute to a decrease in the rate of the
263 reaction catalyzed by these enzymes.

264 Carbapenem hydrolysis by M β LS of the three subclasses takes place by a branched
265 mechanism with two anionic intermediate species (EI¹ and EI², Fig. 6A) (33, 34, 52). Both
266 species are productive, but the final product and the nature of the proton donor differ. EI¹ is
267 the first intermediate produced, absorbs at 390-375 nm (in the case of imipenem and
268 meropenem hydrolysis by NDM-1, respectively), and its N-protonation is produced by a
269 water molecule bridging the Zn(II) ions (33). This species could give rise either to product or
270 to a second intermediate species, EI². This second intermediate species absorbs at 340-
271 336 nm (for imipenem and meropenem, respectively) and is later protonated by a bulk
272 water molecule (not bound to the metal site) leading to the formation of an EP complex
273 lacking a metal-bound water and, later, to a product stereoselectively protonated at C-2
274 (33).

275 As shown in Fig. 6B, the formation of both reaction intermediates was detected

276 during the hydrolysis of imipenem catalyzed by NDM-1 and the L3IMP variant, being more
277 abundant in the second case. However, in the reaction catalyzed by L3VIM or L3Pro, we
278 could not detect the accumulation of any of those intermediates, indicating that the
279 protonation occurred too fast for the species to accumulate to a detectable amount. As
280 accumulation of EI¹ also depends on the formation and consumption of EI², the decrease on
281 the accumulation of the first intermediate species could be due only to an alteration of the
282 protonation rate of EI², by a bulk water molecule. For meropenem hydrolysis the formation
283 of both reaction intermediates was detected with NDM-1 and the L3IMP variant, being,
284 again, more abundant in the second case (Fig. 6C). On the contrary, the hydrolysis by
285 L3VIM and L3Pro evidenced accumulation of only one intermediate (EI¹ in L3VIM and EI² in
286 L3Pro), and to a minor extent than in the wild type enzyme (Fig. 6C). As these results
287 resemble the pattern observed for imipenem, we conclude that these data evidence a
288 general behavior for the hydrolysis of carbapenems (33). Our observations correlate with
289 the steady state parameters for carbapenems where k_{cat} values in L3IMP were lower than
290 the ones of wild type NDM-1, indicating that the reaction rate is diminished, probably due to
291 a decrease in the protonation rate. L3VIM and L3Pro present higher k_{cat} values for
292 carbapenems, correlating with the increased protonation rate.

293

294 DISCUSSION

295 A series of experimental studies of the loop L3 in B1 M β LS performed herein have
296 provided critical information on its role, mostly regarding substrate recognition and mobility.
297 Substitutions at this loop in IMP-1, IMP-12, IMP-43, IMP-18 (36), IMP-2 (45) and VIM-31
298 (38) elicited changes in the substrate profile. Moali and coworkers reported changes in the
299 catalytic efficiency of BclI by engineering the loop of IMP-1 (39). However, a definitive

Mobile loop tunes reaction mechanism of metallo- β -lactamases

300 structural description of the effect of the alterations in this loop is not available. An
301 increased mobility of loop L3 in BclI variants was correlated to a broadening in the substrate
302 profile (37). DEER spectroscopy studies in NDM-1 have demonstrated that loop L3 closes
303 over the active site during catalysis, returning to its original position after hydrolysis (53, 54).
304 Theoretical calculations have predicted a correlation between the movement of loop L3 and
305 the catalytic efficiency in IMP-1 and IMP-6 (55, 56). NMR studies have described in detail
306 the flexibility of loop L3 in different B1 enzymes (37, 57-59), while crystal structures of
307 enzyme-inhibitor or enzyme-product adducts have pointed out how this loop reacts upon
308 small molecule binding to the active site of these M β Ls (5-7, 44, 45, 58-62). Here we show
309 that loop replacement in the scaffold of NDM-1 gives rise to stable, folded proteins, and
310 does not shape the substrate profile of this enzyme. Instead, loop engineering affects the
311 catalytic mechanism, governing the accumulation of key reaction intermediates based on its
312 conformation.

313 Loop replacement induced distinct levels of destabilization in the NDM-1 scaffold.
314 Surprisingly, the largest destabilizing effects *in vitro* were evident in the apo (non-
315 metallated) variants, particularly in L3VIM. The destabilization induced in this variant also
316 correlates with a decreased affinity of the protein toward Zn(II), a higher sensitivity to Zn(II)
317 deprivation in bacteria, and lower expression levels. Some of us have recently reported
318 that, under conditions of Zn(II) deprivation, soluble periplasmic M β Ls are degraded in the
319 apo forms (23). Our previous results account for the link between the reduced Zn(II) affinity
320 and the phenotype observed in the case of L3VIM. Overall, these data highlight the role of
321 Zn(II) binding for the stabilization of M β Ls.

322 The crystal structures and spectroscopic data point to a structurally conserved metal
323 site, with a minor perturbation in the DCH site. Although crystals for the L3VIM variant could

324 not be obtained, the good agreement of Co(II)-substitution experiments with the crystal
325 structures allow us to extrapolate the spectroscopic results on this variant with confidence
326 to the native Zn(II) enzyme. We therefore expect the metal site in L3VIM to be less
327 perturbed compared to NDM-1. Under this assumption, the observed changes could be
328 attributed to changes in loop L3, as observed for the other two variants.

329 Major changes in the reported structures in this analysis are related to the conformation
330 of the engineered loops (Fig. 4). Importantly, our results show that different loops can adopt
331 a wide range of conformations within a given M β L scaffold and reveal details on how the
332 loop L3 sequence defines its conformation. The loop L3 in IMP-1 is closer to the one
333 observed in the engineered L3IMP in the NDM scaffold, while inhibitor binding to IMP-1
334 does not alter the loop conformation as here reported. The same holds for NDM-1, for
335 which inhibitor binding (bisthiazolidines or captopril) does not affect the loop conformation
336 as much as loop engineering does (5-7, 44, 60). We conclude that the loop L3 sequence
337 (regardless of the M β L scaffold) strongly determines its conformation.

338 The catalytic performances of the engineered variants do not reveal a substantial
339 change in the substrate profile of NDM-1. Instead, we report a significant impact on the
340 catalytic mechanism as witnessed by changes in the accumulation of reaction intermediates
341 in the hydrolysis of nitrocefin, imipenem and meropenem. The stability of these reaction
342 intermediates depends on electrostatic interactions with the metal ions, particularly with the
343 DCH site (33, 34, 63, 64) and it has been shown that subtle changes on the M β L active site
344 could tune the stability of these species (26, 63, 65-68). However, the structure of the
345 catalytic Zn(II) center is not perturbed by loop replacement, indicating that other structural
346 features modulate the half-life time of the intermediate species.

347 The conformation of loop L3 directly affects the stability of these intermediates: a more
348 closed loop (as in L3IMP) leads to an enhanced accumulation of the intermediate, while a
349 more open active site (such as in L3Pro) decreases the amount of intermediate (Fig. 6). As
350 the half-life of the anionic reaction intermediates depends on their protonation rates (33,
351 64), these results suggest that the protonation step could be modulated by the solvent
352 accessibility in the different mutants. This also suggests that it is likely that the presence of
353 residues in loop L3 that favor interactions with active site residues (such as Trp64 in L3IMP)
354 could disfavor water accessibility, making the protonation process less effective. We cannot
355 discard the presence of specific interactions of loop L3 with the intermediate species that
356 may increase its stability. This effect may account for the lower k_{cat} values observed for this
357 variant for carbapenem hydrolysis. Overall, these findings show that loop L3 plays an
358 important role in the mechanism of β -lactam hydrolysis by M β Ls by tuning the rate of the
359 rate-limiting step and controlling the accumulation of key reaction intermediates according
360 to its conformation.

361

362 MATERIALS AND METHODS

363 Bacterial Strains and Cloning

364 *Escherichia coli* DH5 α was used for construction and expression of plasmid pMBLe, as
365 well as for all microbiological and biochemical studies. pET26-*bla*_{NDM-1} was kindly provided
366 by Dr. James Spencer (University of Bristol, UK). The construction of pMBLe*bla*_{NDM-1} has
367 been described previously (23) and the same procedure was used for variants cloning. The
368 full-length *bla*_{NDM-1} gene (including its native peptide leaders) was amplified with addition of
369 a C-terminal Strep-tag sequence (for comparative protein detection and quantification), and
370 subcloned into the pMBLe plasmid. The expression of *bla* was induced by the addition of

371 100 μ M IPTG. Addition of the Strep-tag at the C-terminus does not affect MBL ability to
372 confer resistance (23).

373 **Construction of the L3 variants**

374 *bla*_{NVIM}, *bla*_{NIMP} and *bla*_{NP10} containing the *bla*_{NDM-1} gene with the loop L3 of VIM-2, IMP-
375 1 and a Pro residue introduced at the base of the loop, respectively, were custom
376 synthesized (Celtek Genes). The region exchanged comprised residues between Ser57
377 and Ala68 of the NDM-1 structure.

378 **M β L Detection**

379 M β L expression was measured by immunoblotting of cell extracts as described
380 previously (23). Briefly, 5 mL cultures of *E. coli* DH5 α cells carrying the pMBLe *bla*_{NDM-1},
381 *bla*_{NVIM}, *bla*_{NIMP}, and *bla*_{NPRO} plasmids were grown aerobically at 37 °C in LB broth with 20
382 μ g/ml gentamicin to log phase (OD_{600nm} = 0.4). M β L expression was then induced with 100
383 μ M IPTG, and cultures were left to grow to an OD₆₀₀ of 1. Cultures were pelleted and cells
384 were washed once with 20 mM Tris, 150 mM NaCl, pH 8.0. An aliquot of cell crude extract
385 were separated on this step. The rest of the washed cells were pelleted again and were
386 resuspended in 20 mM Tris, 0.1 mM EDTA, 20% w/v sucrose, 1 mg/mL lysozyme (from
387 chicken egg white, Sigma-Aldrich, protein \geq 90%), 0.5 mM PMSF, pH 8 (resuspension
388 volume was normalized based on OD_{600nm}). The cells were incubated with agitation at 4°C
389 for 30 min. The cells were pelleted and the periplasmic extract was obtaining in the
390 supernatant. The pellet consisting of spheroplasts was washed in 20 mM Tris, 0.1 mM
391 EDTA, 20% w/v sucrose, pH 8 and resuspended in the same volume of this buffer. A total
392 of 120 μ L of the different extracts were mixed with 30 μ L loading dye and separated by
393 SDS-PAGE (10 μ L of whole cells lysate, 25 μ L spheroplasts and 25 μ L periplasmic
394 extracts) and transferred to a polyvinylidene difluoride membrane (Novex, Life

395 Technologies, Carlsbad, CA) by electroblotting. Strep-Tag® II monoclonal antibodies (at
396 1:1000 dilution from 200 μ g/ml solution, Novagen) and immunoglobulin G-alkaline
397 phosphatase conjugates (at 1:3000 dilution) were used to detect M β L expression. GroEL
398 and MPB antibodies were added as loading controls. Protein band intensities were
399 quantified from PVDF membranes with ImageJ software (69).

400 **Cell-Based Assays**

401 To test the phenotypic effect of the loop L3 substitutions, the minimal inhibitory
402 concentrations (MICs) of piperacillin, ceftazidime, cefotaxime, cefepime, imipenem, and
403 meropenem were determined for each clone in the LB medium using the agar macrodilution
404 method according to CLSI guidelines (70). Protein expression was induced with 100 μ M
405 IPTG, except for ceftazidime where induction was performed with 20 μ M IPTG. In order to
406 measure the effect of Zn(II) availability on antibiotic resistance, the growth medium was
407 supplemented with varying concentrations of the metal chelator dipicolinic acid (DPA,
408 Merck, >98%). In all cases, plasmid expression was induced with 100 μ M IPTG (71). An
409 extra measurement was performed with 500 μ M of ZnSO₄ to reach the maximum activity of
410 the proteins (100%). DPA or ZnSO₄ were added to the LB plate along with gentamicin and
411 IPTG.

412 On the steady-state expression of proteins in cells treated with DPA, after 1 h of
413 induction with 100 μ M IPTG, *E. coli* DH5 α cells expressing the NDM variants were
414 incubated during 15 min with or without 250 μ M DPA. Protein expression was detected from
415 10 μ l of whole cell lysates by western blot, as previously described.

416 **Protein Purification**

417 For kinetic studies, mature M β Ls (residues 39 to 270) were produced in *E. coli* BL21
418 (DE3) and purified as previously published for NDM-1 (5), with the following two
419 modifications. Firstly, LB supplemented with 50 μ g/ml kanamycin was used instead of

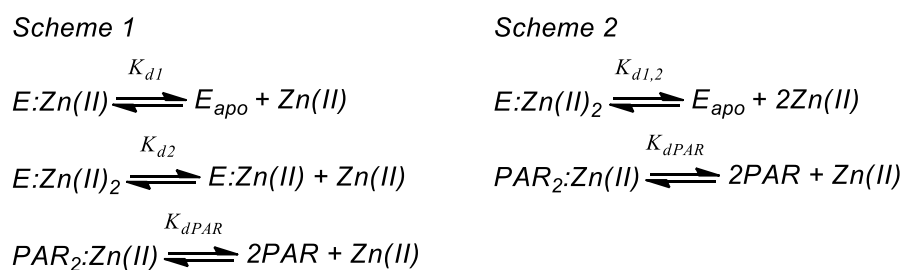
420 minimal media. Secondly, M β L production was induced by addition of 0.25 mM IPTG.
421 Protein concentration was measured spectrophotometrically using $\epsilon_{280} = 27960 \text{ M}^{-1} \text{ cm}^{-1}$ for
422 NDM-1, L3VIM, and L3Pro, and $\epsilon_{280} = 31970 \text{ M}^{-1} \text{ cm}^{-1}$ for L3IMP. Metal content was
423 measured using the colorimetric reagent 4-(2-pyridylazo) resorcinol (PAR) under denaturing
424 conditions (72). The average metal content of the variants were somehow lower (1.5 for
425 L3VIM, 1.6 for L3Pro and 1.65 for L3IMP) compared to the wild type protein (1.8
426 equivalents of Zn(II) per enzyme) (33).

427 **Determination of Zn(II) Affinity Constants**

428 Dissociation constants for Zn(II) were estimated by competition with the chromophoric
429 chelator PAR, as previously described (26). Briefly, PAR is a metallochromic compound,
430 whose UV-Visible absorption spectrum is modified upon metal uptake, as reflected by a
431 shift of its maximum absorption wavelength from 414 to 500 nm. Using the previously
432 published molar absorption coefficients of free PAR ($\epsilon_{\text{PAR}414\text{nm}} = 36868 \pm 1843 \text{ M}^{-1} \text{ cm}^{-1}$;
433 $\epsilon_{\text{PAR}500\text{nm}} = 1289 \pm 65 \text{ M}^{-1} \text{ cm}^{-1}$), PAR-Zn(II) complex ($\epsilon_{\text{PAR}2\text{Zn}414\text{nm}} = 12788 \pm 576 \text{ M}^{-1} \text{ cm}^{-1}$;
434 $\epsilon_{\text{PAR}2\text{Zn}500\text{nm}} = 80000 \pm 4000 \text{ M}^{-1} \text{ cm}^{-1}$) and the disassociation constant (K_d) for the PAR-
435 Zn(II) complex ($2.6 \pm 0.2 \cdot 10^{-12} \text{ M}$), we were able to quantify the amount of PAR at each
436 state in a given sample (73).

437 Disassociation constants for NDM-1 and all the L3 variants were determined at 25 °C
438 by titrations curves on 40 mM MOPS, 0.1 M NaCl, pH 7.3 (previously treated with Chelex)
439 supplemented with 1.5 μM ZnSO₄ and PAR at 3 and 6 μM . Apo enzyme was added at
440 increasing amount at each point, until a final concentration of 3 μM was reached, and the
441 absorption spectra between 300 and 600 nm were recorded. Absorbances at 414 and 500
442 nm were corrected by subtracting the absorbance at 600 nm, which was taken as baseline.
443 Metal binding to wild-type NDM-1, L3VIM and L3IMP could be described by a two-step
444 binding model. Data were fit with DynaFit 3 (Biokin) (74) to the equilibrium shown in

445 Scheme 1; were K_{d1} and K_{d2} are the disassociation constants of the enzyme:Zn(II) complex,
 446 and K_{dPAR} corresponds to the dissociation of the PAR:Zn(II) complex. For the L3Pro variant
 447 a second model with one K_d ($K_{d1,2}$, Table S1) for the enzyme-Zn(II) complex was proposed
 448 (Scheme 2).



449

450 **Steady-state Kinetics**

451 β -Lactamase activity was measured in a JASCO V-670 spectrophotometer at 30 °C in
 452 10 mM HEPES pH 7.5 and 200 mM NaCl supplemented with 20 μ M ZnSO₄ and 20 μ g/mL
 453 bovine serum albumin (BSA). Substrates were used in the μ M range, whereas the enzymes
 454 were used in the nM range in order to ensure pseudo-first-order kinetics. It was only
 455 considered the concentration of metallated protein. The following differential extinction
 456 coefficients were used: nitrocefin, $\Delta\epsilon_{482} = 17400 \text{ M}^{-1} \text{ cm}^{-1}$; PenG, $\Delta\epsilon_{235} = -775 \text{ M}^{-1} \text{ cm}^{-1}$;
 457 piperacillin, $\Delta\epsilon_{235} = -820 \text{ M}^{-1} \text{ cm}^{-1}$; ceftazidime, $\Delta\epsilon_{256} = -7600 \text{ M}^{-1} \text{ cm}^{-1}$; cefepime, $\Delta\epsilon_{260} =$
 458 $-750 \text{ M}^{-1} \text{ cm}^{-1}$; imipenem, $\Delta\epsilon_{300} = -9000 \text{ M}^{-1} \text{ cm}^{-1}$; meropenem, $\Delta\epsilon_{300} = -6,500 \text{ M}^{-1} \text{ cm}^{-1}$;
 459 ertapenem, $\Delta\epsilon_{299} = -9970 \text{ M}^{-1} \text{ cm}^{-1}$.

460 **Stopped-Flow Experiments**

461 The variations in the visible spectra of NDM-1 and its L3 variants during hydrolysis of
 462 nitrocefin, imipenem and meropenem were followed with an Applied Photophysics SX.18-
 463 MVR stopped-flow system associated to a photodiode-array detector (Applied
 464 Photophysics, U.K.). The measurements were performed in 100 mM HEPES, pH 7.5, 200

465 mM NaCl and 0.3 mM ZnSO₄, at 6 °C. Data were corrected for the instrument dead time (2
466 ms). In all cases, a 1:1 ratio of metallated enzyme and substrate was used.

467 **Thermal denaturation assays**

468 Protein stability to thermal denaturation was determined on both holo and apoprotein
469 by using the Protein Thermal Shift™ Assay (Applied Biosystems, Carlsbad, CA), following
470 manufacturer's instructions. Data were fit to a two-step model, as previously described (75).

471 **Preparation of Apo and Co(II) substituted enzymes**

472 The non-metallated forms of Apo-NDM-1, apo-L3VIM, apo-L3IMP, and apo-L3Pro,
473 were prepared by successive dialysis of the purified holoproteins against chelators, as
474 described previously (49). All buffer solutions used to prepare the apoenzymes were treated
475 by extensive stirring with Chelex 100 (Sigma). Metal content of the apoprotein preparations
476 was checked using PAR, as described above. Co(II) substituted enzymes were obtained
477 after titration on apo derivatives with CoSO₄ (49).

478 **X-ray crystallography**

479 The proteins were purified as described before with an additional size-exclusion
480 chromatography step, in final buffer HEPES 10 mM pH 7.5, NaCl 200 mM, and
481 concentrated to 30 mg/ml. Crystals were grown with the hanging-drop vapor diffusion
482 method at 18 °C. Drops were set by mixing equal volumes of protein and reservoir solution.
483 L3IMP crystals were grown in 100 mM HEPES pH 7.55, 0.1 M NaCl, 1.35 M (NH₄)₂SO₄
484 applying microseeding. L3Pro crystals were grown in 100 mM HEPES pH 7.0, 500 mM
485 (NH₄)₂SO₄, 5 mM CoCl₂-NiCl₂-MgCl₂-CdCl₂ and 12-30% (w/v) PEG 3350. All crystals were
486 flash-frozen, either in mother liquor supplemented with 35% glycerol or 50% paraffin oil, and
487 stored in liquid nitrogen.

488 X-ray diffraction data were collected at 100 K at the Proxima 1 beamline (Synchrotron
489 Soleil, Saint-Aubin, France). Data reduction was carried out using XDS (76) and Aimless

490 from the CCP4 program suite (77). The crystal structures of both proteins were solved by
491 molecular replacement using the programs Molrep (78) or Phaser (79) and a previously
492 determined NDM-1 structure (PDB entry 3SPU, chain C) as search probe. The final
493 crystallographic models were obtained through iterative rounds of refinement with Buster
494 (80) and manual rebuilding with COOT (81). Data collection and refinement statistics are
495 summarized in Table S4. Both crystallographic models were validated with MolProbity (82)
496 and the rmsd calculations were performed with PDBeFold (83). Illustrations were made with
497 PyMOL (Schrödinger, New York, USA).

498 To ascertain the presence of Zn metal ions in the active site of L3Pro crystals, two
499 complete datasets were collected at the ESRF beamline id23eh1 using X-ray wavelengths
500 immediately above (hr, $\lambda=1.27241$ Å) and below (lr, $\lambda=1.28348$ Å) the Zn K-edge as
501 determined with a fluorescence scan. Using phases from the refined protein model, double
502 difference anomalous maps (Dano(hr) – Dano(lr)) were produced with the programs
503 SFTOOLS and FFT from the CCP4 suite (77) (Supplementary Figure 4). The presence of
504 Ni(II) ions (from the crystallization buffer) mediating protein-protein interactions in L3Pro
505 was confirmed in a similar way (hr, $\lambda=1.48030$ Å; lr, $\lambda=1.48840$ Å). In all cases, data
506 processing and reduction were carried out as described before (Table S4).

507

508 **Accession numbers**

509 Structural data are available in Protein Data Bank database under the accession codes
510 6C6I (L3IMP) and 6CAC (L3Pro).

511

512 **Acknowledgments:** A.R.P. and E.G. were recipients of doctoral fellowships from
513 CONICET. M.F.M. was recipient of doctoral scholarship from COLCIENCIAS. L.H.O., S.K.,

514 L.I.L. and A.J.V. are staff members from CONICET. This work was supported by grants
515 from ANPCyT (A.J.V.), NIH R01 AI100560 (A.J.V. and R.A.B), NIH R01 AI063517, and R01
516 AI072219 (R.A.B.), ECOS-MinCyT collaborative project (A.J.V. and P.M.A), Cleveland
517 Department of Veterans Affairs 1I01BX001974 (R.A.B.) and Development and the Geriatric
518 Research Education and Clinical Center (R.A.B.). The content is solely the responsibility of
519 the authors and does not necessarily represent the official views of the National Institutes of
520 Health or the Department of Veterans Affairs. The funders had no role in study design, data
521 collection and interpretation, or the decision to submit the work for publication. We thank
522 Ahmed Haouz and Patrick Weber (Institut Pasteur) for their help with robot-driven
523 crystallization screenings. We acknowledge the synchrotron sources Soleil (Saint-Aubin,
524 France) and ESRF (Grenoble, France) for granting access to their facilities, and their staff
525 members for the helpful assistance.

526

527 **Author Contributions:** A.R.P. and M.F.M. purified protein samples, performed the
528 biochemical characterization of the proteins and performed and analyzed the activity
529 measurements and stopped-flow experiments. E.G. crystallized the proteins, collected the
530 X-ray diffraction data and solved the structures. S.K., L.H.O. and P.M.A. performed data
531 collection and resolution of the X-ray structures. M.A.T. and C.R.B. helped with the
532 construction of the protein variants. E.G., S.K., L.H.O. and P.A.M. analyzed and discussed
533 the crystallographic data. A.R.P., M.F.M., R.A.B., L.I.L., and A.J.V. analyzed and discussed
534 the data. A.R.P., M.F.M., E.G. and A.J.V. wrote the paper, and all authors discussed the
535 results and commented on the manuscript.

536

537 **Conflict of interest:** The authors declare that they have no conflicts of interest with the
538 contents of this article.

539

540 **Abbreviations:** M β Ls, metallo- β -lactamases; NDM, New Delhi metallo- β -lactamase; VIM,
541 Verona integron–encoded metallo- β -lactamase; IMP, Imipenemase metallo- β -lactamase;
542 MIC, minimum inhibitory concentration; DPA, dipicolinic acid; PAR, 4-(2-pyridylazo)
543 resorcinol; LMCT, ligand-to-metal charge-transfer (LMCT); PDA, photodiode array; rmsd,
544 root mean square deviation; DEER, double electron electron resonance, PDA, photodiode
545 array detector.

546

547 **Keywords:** metallo- β -lactamase, antibiotic resistance, New Delhi metallo- β -lactamase,
548 enzyme mechanism, enzyme structure.

549

550

References

551

552 1. Fisher JF, Meroueh SO, Mobashery S. 2005. Bacterial resistance to beta-lactam
553 antibiotics: compelling opportunism, compelling opportunity. *Chem Rev* 105:395-424.

554 2. Bonomo RA, Tolmasky M. 2007. Enzyme-mediated resistance to antibiotics:
555 mechanisms, dissemination, and prospects for inhibition. Enzyme-mediated
556 resistance to antibiotics: mechanisms, dissemination, and prospects for inhibition.

557 3. Bush K, Jacoby GA. 2010. Updated functional classification of β -lactamases.
558 *Antimicrobial Agents and chemotherapy* 54:969-976.

559 4. King AM, Reid-Yu SA, Wang W, King DT, De Pascale G, Strynadka NC, Walsh TR,
560 Coombes BK, Wright GD. 2014. Aspergillomarasmine A overcomes metallo-beta-
561 lactamase antibiotic resistance. *Nature* 510:503-6.

562 5. Gonzalez MM, Kosmopoulou M, Mojica MF, Castillo V, Hinchliffe P, Pettinati I, Brem
563 J, Schofield CJ, Mahler G, Bonomo RA, Llarrull LI, Spencer J, Vila AJ. 2015.
564 Bisthiazolidines: A Substrate-Mimicking Scaffold as an Inhibitor of the NDM-1
565 Carbapenemase. *ACS Infect Dis* 1:544-54.

566 6. Hinchliffe P, González MM, Mojica MF, González JM, Castillo V, Saiz C,
567 Kosmopoulou M, Tooke CL, Llarrull LI, Mahler G, Bonomo RA, Vila AJ, Spencer J.
568 2016. Cross-class metallo- β -lactamase inhibition by bisthiazolidines reveals multiple
569 binding modes. *Proceedings of the National Academy of Sciences* 113:E3745-
570 E3754.

571 7. Mojica MF, Mahler SG, Bethel CR, Taracila MA, Kosmopoulou M, Papp-Wallace KM,
572 Llarrull LI, Wilson BM, Marshall SH, Wallace CJ. 2015. Exploring the role of residue
573 228 in substrate and inhibitor recognition by VIM metallo- β -lactamases. *Biochemistry*
574 54:3183-3196.

- 575 8. Brem J, Cain R, Cahill S, McDonough MA, Clifton IJ, Jimenez-Castellanos JC,
576 Avison MB, Spencer J, Fishwick CW, Schofield CJ. 2016. Structural basis of metallo-
577 beta-lactamase, serine-beta-lactamase and penicillin-binding protein inhibition by
578 cyclic boronates. *Nat Commun* 7:12406.
- 579 9. Everett M, Sprynski N, Coelho A, Castandet J, Bayet M, Bougnon J, Lozano C,
580 Davies DT, Leiris S, Zalacain M. 2018. Discovery of a Novel Metallo- β -Lactamase
581 Inhibitor, which can Potentiate Meropenem Activity against Carbapenem-Resistant
582 Enterobacteriaceae. *Antimicrobial Agents and Chemotherapy*:AAC. 00074-18.
- 583 10. Hinchliffe P, Tanner CA, Krismanich AP, Labbé Gv, Goodfellow VJ, Marrone L,
584 Desoky AY, Calvopiña K, Whittle EE, Zeng F. 2018. Structural and Kinetic Studies of
585 the Potent Inhibition of Metallo- β -lactamases by 6-Phosphonomethylpyridine-2-
586 carboxylates. *Biochemistry*.
- 587 11. Sevaille L, Gavara L, Bebrone C, De Luca F, Nauton L, Achard M, Mercuri P,
588 Tanfoni S, Borgianni L, Guyon C. 2017. 1, 2, 4 - Triazole - 3 - thione compounds as
589 inhibitors of di - zinc metallo - β - lactamases. *ChemMedChem*.
- 590 12. Wang R, Lai T-P, Gao P, Zhang H, Ho P-L, Woo PC-Y, Ma G, Kao RY-T, Li H, Sun
591 H. 2018. Bismuth antimicrobial drugs serve as broad-spectrum metallo- β -lactamase
592 inhibitors. *Nature communications* 9:439.
- 593 13. Bebrone C. 2007. Metallo- β -lactamases (classification, activity, genetic organization,
594 structure, zinc coordination) and their superfamily. *Biochemical pharmacology*
595 74:1686-1701.
- 596 14. Cornaglia G, Giamarellou H, Rossolini GM. 2011. Metallo- β -lactamases: a last
597 frontier for β -lactams? *The Lancet infectious diseases* 11:381-393.

- 598 15. Crowder MW, Spencer J, Vila AJ. 2006. Metallo-beta-lactamases: novel weaponry
599 for antibiotic resistance in bacteria. *Acc Chem Res* 39:721-8.
- 600 16. Mojica MF, Bonomo RA, Fast W. 2016. B1-Metallo-beta-Lactamases: Where Do We
601 Stand? *Curr Drug Targets* 17:1029-50.
- 602 17. Olsen I. 2015. New promising β -lactamase inhibitors for clinical use. *European*
603 *Journal of Clinical Microbiology & Infectious Diseases* 34:1303-1308.
- 604 18. Rotondo CM, Wright GD. 2017. Inhibitors of metallo-beta-lactamases. *Curr Opin*
605 *Microbiol* 39:96-105.
- 606 19. Bonomo RA. 2017. Beta-Lactamases: A Focus on Current Challenges. *Cold Spring*
607 *Harb Perspect Med* 7.
- 608 20. Ma Z, Jacobsen FE, Giedroc DP. 2009. Coordination chemistry of bacterial metal
609 transport and sensing. *Chem Rev* 109:4644-81.
- 610 21. Meini MR, Llarrull LI, Vila AJ. 2015. Overcoming differences: The catalytic
611 mechanism of metallo-beta-lactamases. *FEBS Lett* 589:3419-32.
- 612 22. Palzkill T. 2013. Metallo-beta-lactamase structure and function. *Ann N Y Acad Sci*
613 1277:91-104.
- 614 23. Gonzalez LJ, Bahr G, Nakashige TG, Nolan EM, Bonomo RA, Vila AJ. 2016.
615 Membrane anchoring stabilizes and favors secretion of New Delhi metallo-beta-
616 lactamase. *Nat Chem Biol* 12:516-22.
- 617 24. Bonomo RA. 2011. New Delhi metallo- β -lactamase and multidrug resistance: a
618 global SOS? *Clinical Infectious Diseases* 52:485-487.
- 619 25. Johnson AP, Woodford N. 2013. Global spread of antibiotic resistance: the example
620 of New Delhi metallo- β -lactamase (NDM)-mediated carbapenem resistance. *Journal*
621 *of medical microbiology* 62:499-513.

- 622 26. Gonzalez JM, Meini MR, Tomatis PE, Medrano Martin FJ, Cricco JA, Vila AJ. 2012.
623 Metallo-beta-lactamases withstand low Zn(II) conditions by tuning metal-ligand
624 interactions. *Nat Chem Biol* 8:698-700.
- 625 27. Jacquin O, Balbeur D, Damblon C, Marchot P, De Pauw E, Roberts GC, Frere JM,
626 Matagne A. 2009. Positively cooperative binding of zinc ions to *Bacillus cereus*
627 569/H/9 beta-lactamase II suggests that the binuclear enzyme is the only relevant
628 form for catalysis. *J Mol Biol* 392:1278-91.
- 629 28. Garau G, Garcia-Saez I, Bebrone C, Anne C, Mercuri P, Galleni M, Frere JM,
630 Dideberg O. 2004. Update of the standard numbering scheme for class B beta-
631 lactamases. *Antimicrob Agents Chemother* 48:2347-9.
- 632 29. Orellano EG, Girardini JE, Cricco JA, Ceccarelli EA, Vila AJ. 1998. Spectroscopic
633 characterization of a binuclear metal site in *Bacillus cereus* beta-lactamase II.
634 *Biochemistry* 37:10173-80.
- 635 30. Concha NO, Rasmussen BA, Bush K, Herzberg O. 1996. Crystal structure of the
636 wide-spectrum binuclear zinc β -lactamase from *Bacteroides fragilis*. *Structure* 4:823-
637 836.
- 638 31. Carfi A, Paul-Soto R, Martin L, Petillot Y, Frère J-M, Dideberg O. 1997. Purification,
639 crystallization and preliminary X-ray analysis of *Bacteroides fragilis* Zn²⁺ β -
640 lactamase. *Acta Crystallographica Section D: Biological Crystallography* 53:485-487.
- 641 32. Yang H, Aitha M, Hetrick AM, Richmond TK, Tierney DL, Crowder MW. 2012.
642 Mechanistic and spectroscopic studies of metallo-beta-lactamase NDM-1.
643 *Biochemistry* 51:3839-47.
- 644 33. Lisa MN, Palacios AR, Aitha M, Gonzalez MM, Moreno DM, Crowder MW, Bonomo
645 RA, Spencer J, Tierney DL, Llarrull LI, Vila AJ. 2017. A general reaction mechanism

- 646 for carbapenem hydrolysis by mononuclear and binuclear metallo-beta-lactamases.
647 Nat Commun 8:538.
- 648 34. Tioni MF, Llarrull LI, Poeylout-Palena AA, Marti MA, Saggiu M, Periyannan GR, Mata
649 EG, Bennett B, Murgida DH, Vila AJ. 2008. Trapping and characterization of a
650 reaction intermediate in carbapenem hydrolysis by *B. cereus* metallo-beta-
651 lactamase. J Am Chem Soc 130:15852-63.
- 652 35. Materon IC, Beharry Z, Huang W, Perez C, Palzkill T. 2004. Analysis of the context
653 dependent sequence requirements of active site residues in the metallo-beta-
654 lactamase IMP-1. J Mol Biol 344:653-63.
- 655 36. Furuyama T, Nonomura H, Ishii Y, Hanson ND, Shimizu-Ibuka A. 2016. Structural
656 and Mutagenic Analysis of Metallo-beta-Lactamase IMP-18. Antimicrob Agents
657 Chemother 60:5521-6.
- 658 37. Gonzalez MM, Abriata LA, Tomatis PE, Vila AJ. 2016. Optimization of
659 Conformational Dynamics in an Epistatic Evolutionary Trajectory. Mol Biol Evol
660 33:1768-76.
- 661 38. Kupper MB, Herzog K, Bennink S, Schlomer P, Bogaerts P, Glupczynski Y, Fischer
662 R, Bebrone C, Hoffmann KM. 2015. The three-dimensional structure of VIM-31--a
663 metallo-beta-lactamase from *Enterobacter cloacae* in its native and oxidized form.
664 FEBS J 282:2352-60.
- 665 39. Moali C, Anne C, Lamotte-Brasseur J, Gros Lambert S, Devreese B, Van Beeumen J,
666 Galleni M, Frere JM. 2003. Analysis of the importance of the metallo-beta-lactamase
667 active site loop in substrate binding and catalysis. Chem Biol 10:319-29.
- 668 40. LaCuran AE, Pegg KM, Liu EM, Bethel CR, Ai N, Welsh WJ, Bonomo RA,
669 Oelschlaeger P. 2015. Elucidating the Role of Residue 67 in IMP-Type Metallo-beta-
670 Lactamase Evolution. Antimicrob Agents Chemother 59:7299-307.

- 671 41. Green VL, Verma A, Owens RJ, Phillips SE, Carr SB. 2011. Structure of New Delhi
672 metallo-beta-lactamase 1 (NDM-1). *Acta Crystallogr Sect F Struct Biol Cryst*
673 *Commun* 67:1160-4.
- 674 42. Guo Y, Wang J, Niu G, Shui W, Sun Y, Zhou H, Zhang Y, Yang C, Lou Z, Rao Z.
675 2011. A structural view of the antibiotic degradation enzyme NDM-1 from a
676 superbug. *Protein & cell* 2:384-394.
- 677 43. King D, Strynadka N. 2011. Crystal structure of New Delhi metallo-beta-lactamase
678 reveals molecular basis for antibiotic resistance. *Protein Sci* 20:1484-91.
- 679 44. King DT, Worrall LJ, Gruninger R, Strynadka NC. 2012. New Delhi metallo-beta-
680 lactamase: structural insights into beta-lactam recognition and inhibition. *J Am Chem*
681 *Soc* 134:11362-5.
- 682 45. Yamaguchi Y, Matsueda S, Matsunaga K, Takashio N, Toma-Fukai S, Yamagata Y,
683 Shibata N, Wachino J, Shibayama K, Arakawa Y, Kurosaki H. 2015. Crystal structure
684 of IMP-2 metallo-beta-lactamase from *Acinetobacter* spp.: comparison of active-site
685 loop structures between IMP-1 and IMP-2. *Biol Pharm Bull* 38:96-101.
- 686 46. Zhang H, Hao Q. 2011. Crystal structure of NDM-1 reveals a common β -lactam
687 hydrolysis mechanism. *The FASEB Journal* 25:2574-2582.
- 688 47. Morán-Barrio J, Limansky AS, Viale AM. 2009. Secretion of GOB metallo- β -
689 lactamase in *Escherichia coli* depends strictly on the cooperation between the
690 cytoplasmic DnaK chaperone system and the Sec machinery: completion of folding
691 and Zn (II) ion acquisition occur in the bacterial periplasm. *Antimicrobial agents and*
692 *chemotherapy* 53:2908-2917.
- 693 48. Neumann W, Gulati A, Nolan EM. 2017. Metal homeostasis in infectious disease:
694 recent advances in bacterial metallophores and the human metal-withholding
695 response. *Curr Opin Chem Biol* 37:10-18.

Mobile loop tunes reaction mechanism of metallo- β -lactamases

- 696 49. Llarrull LI, Tioni MF, Kowalski J, Bennett B, Vila AJ. 2007. Evidence for a dinuclear
697 active site in the metallo-beta-lactamase BclI with substoichiometric Co(II). A new
698 model for metal uptake. *J Biol Chem* 282:30586-95.
- 699 50. Wang Z, Fast W, Benkovic SJ. 1998. Direct Observation of an Enzyme-Bound
700 Intermediate in the Catalytic Cycle of the Metallo- β -Lactamase from *Bacteroides*
701 *fragilis*. *Journal of the American Chemical Society* 120:10788-10789.
- 702 51. Thomas PW, Zheng M, Wu S, Guo H, Liu D, Xu D, Fast W. 2011. Characterization of
703 purified New Delhi metallo-beta-lactamase-1. *Biochemistry* 50:10102-13.
- 704 52. Brem J, Struwe WB, Rydzik AM, Tarhonskaya H, Pfeffer I, Flashman E, van Berkel
705 SS, Spencer J, Claridge TD, McDonough MA, Benesch JL, Schofield CJ. 2015.
706 Studying the active-site loop movement of the Sao Paulo metallo-beta-lactamase-1.
707 *Chem Sci* 6:956-963.
- 708 53. Aitha M, Moritz L, Sahu ID, Sanyurah O, Roche Z, McCarrick R, Lorigan GA, Bennett
709 B, Crowder MW. 2015. Conformational dynamics of metallo-beta-lactamase CcrA
710 during catalysis investigated by using DEER spectroscopy. *J Biol Inorg Chem*
711 20:585-94.
- 712 54. Aitha M, Moller AJ, Sahu ID, Horitani M, Tierney DL, Crowder MW. 2016.
713 Investigating the position of the hairpin loop in New Delhi metallo-beta-lactamase,
714 NDM-1, during catalysis and inhibitor binding. *J Inorg Biochem* 156:35-9.
- 715 55. Oelschlaeger P, Mayo SL. 2005. Hydroxyl Groups in the $\beta\beta$ Sandwich of Metallo- β -
716 lactamases Favor Enzyme Activity: A Computational Protein Design Study. *Journal*
717 *of Molecular Biology* 350:395-401.
- 718 56. Oelschlaeger P, Schmid RD, Pleiss J. 2003. Modeling domino effects in enzymes:
719 molecular basis of the substrate specificity of the bacterial metallo-beta-lactamases
720 IMP-1 and IMP-6. *Biochemistry* 42:8945-56.

Mobile loop tunes reaction mechanism of metallo- β -lactamases

- 721 57. Abboud MI, Hinchliffe P, Brem J, Macsics R, Pfeffer I, Makena A, Umland KD,
722 Rydzik AM, Li GB, Spencer J, Claridge TD, Schofield CJ. 2017. (19) F-NMR Reveals
723 the Role of Mobile Loops in Product and Inhibitor Binding by the Sao Paulo Metallo-
724 beta-Lactamase. *Angew Chem Int Ed Engl* 56:3862-3866.
- 725 58. Rydzik AM, Brem J, van Berkel SS, Pfeffer I, Makena A, Claridge TD, Schofield CJ.
726 2014. Monitoring conformational changes in the NDM-1 metallo-beta-lactamase by
727 ¹⁹F NMR spectroscopy. *Angew Chem Int Ed Engl* 53:3129-33.
- 728 59. Scrofani SD, Chung J, Huntley JJ, Benkovic SJ, Wright PE, Dyson HJ. 1999. NMR
729 characterization of the metallo-beta-lactamase from *Bacteroides fragilis* and its
730 interaction with a tight-binding inhibitor: role of an active-site loop. *Biochemistry*
731 38:14507-14.
- 732 60. Brem J, van Berkel SS, Zollman D, Lee SY, Gileadi O, McHugh PJ, Walsh TR,
733 McDonough MA, Schofield CJ. 2015. Structural Basis of Metallo-beta-Lactamase
734 Inhibition by Captopril Stereoisomers. *Antimicrob Agents Chemother* 60:142-50.
- 735 61. Huntley JJ, Fast W, Benkovic SJ, Wright PE, Dyson HJ. 2003. Role of a solvent-
736 exposed tryptophan in the recognition and binding of antibiotic substrates for a
737 metallo-beta-lactamase. *Protein Sci* 12:1368-75.
- 738 62. Huntley JJ, Scrofani SD, Osborne MJ, Wright PE, Dyson HJ. 2000. Dynamics of the
739 metallo- β -lactamase from *Bacteroides fragilis* in the presence and absence of a tight-
740 binding inhibitor. *Biochemistry* 39:13356-13364.
- 741 63. Yang H, Aitha M, Marts AR, Hetrick A, Bennett B, Crowder MW, Tierney DL. 2014.
742 Spectroscopic and mechanistic studies of heterodimetallic forms of metallo-beta-
743 lactamase NDM-1. *J Am Chem Soc* 136:7273-85.
- 744 64. Tripathi R, Nair NN. 2015. Mechanism of Meropenem Hydrolysis by New Delhi
745 Metallo β -Lactamase. *ACS Catalysis* 5:2577-2586.

- 746 65. Gallagher SR. 2001. One-Dimensional Electrophoresis Using Nondenaturing
747 Conditions. doi:10.1002/0471140864.ps1003s00:10.3.1-10.3.11.
- 748 66. Llarrull LI, Fabiane SM, Kowalski JM, Bennett B, Sutton BJ, Vila AJ. 2007. Asp-120
749 locates Zn²⁺ for optimal metallo-beta-lactamase activity. *J Biol Chem* 282:18276-85.
- 750 67. Tomatis PE, Fabiane SM, Simona F, Carloni P, Sutton BJ, Vila AJ. 2008. Adaptive
751 protein evolution grants organismal fitness by improving catalysis and flexibility. *Proc*
752 *Natl Acad Sci U S A* 105:20605-10.
- 753 68. Gonzalez JM, Medrano Martin FJ, Costello AL, Tierney DL, Vila AJ. 2007. The Zn²⁺
754 position in metallo-beta-lactamases is critical for activity: a study on chimeric metal
755 sites on a conserved protein scaffold. *J Mol Biol* 373:1141-56.
- 756 69. Schneider CA, Rasband WS, Eliceiri KW. 2012. NIH Image to ImageJ: 25 years of
757 image analysis. *Nat Methods* 9:671-5.
- 758 70. Clinical and Laboratory Standards Institute. 2016. Performance Standards for
759 Antimicrobial Susceptibility Testing. 26th Ed. CLSI Supplement M100S. Wayne, PA.
- 760 71. Bahr G, Vitor-Horen L, Bethel CR, Bonomo RA, Gonzalez LJ, Vila AJ. 2017. Clinical
761 evolution of New Delhi Metallo-beta-lactamase (NDM) optimizes resistance under
762 Zn(II) deprivation. *Antimicrob Agents Chemother* doi:10.1128/AAC.01849-17.
- 763 72. Hunt JB, Neece SH, Ginsburg A. 1985. The use of 4-(2-pyridylazo)resorcinol in
764 studies of zinc release from *Escherichia coli* aspartate transcarbamoylase. *Anal*
765 *Biochem* 146:150-7.
- 766 73. Skagseth S, Carlsen TJ, Bjerga GEK, Spencer J, Samuelsen Ø, Leiros H-KS. 2016.
767 Role of Residues W228 and Y233 in the Structure and Activity of Metallo- β -
768 Lactamase GIM-1. *Antimicrobial agents and chemotherapy* 60:990-1002.
- 769 74. Kuzmic P. 1996. Program DYNAFIT for the analysis of enzyme kinetic data:
770 application to HIV proteinase. *Anal Biochem* 237:260-73.

- 771 75. Huynh K, Partch CL. 2015. Analysis of protein stability and ligand interactions by
772 thermal shift assay. *Curr Protoc Protein Sci* 79:28 9 1-14.
- 773 76. Kabsch W. 2010. Xds. *Acta Crystallogr D Biol Crystallogr* 66:125-32.
- 774 77. Winn MD, Ballard CC, Cowtan KD, Dodson EJ, Emsley P, Evans PR, Keegan RM,
775 Krissinel EB, Leslie AG, McCoy A, McNicholas SJ, Murshudov GN, Pannu NS,
776 Potterton EA, Powell HR, Read RJ, Vagin A, Wilson KS. 2011. Overview of the
777 CCP4 suite and current developments. *Acta Crystallogr D Biol Crystallogr* 67:235-42.
- 778 78. Vagin A, Teplyakov A. 2010. Molecular replacement with MOLREP. *Acta Crystallogr*
779 *D Biol Crystallogr* 66:22-5.
- 780 79. McCoy AJ, Grosse-Kunstleve RW, Adams PD, Winn MD, Storoni LC, Read RJ.
781 2007. Phaser crystallographic software. *J Appl Crystallogr* 40:658-674.
- 782 80. Bricogne G, Blanc E, Brandl M, Flensburg C, Kelle P, Paciorek P, Roversi P, Sharff
783 A, Smart O, Vonrhein C, Womack T. 2010. BUSTER version 2.9., United Kingdom:
784 Global Phasing Ltd. , Cambridge.
- 785 81. Emsley P, Cowtan K. 2004. Coot: model-building tools for molecular graphics. *Acta*
786 *Crystallogr D Biol Crystallogr* 60:2126-32.
- 787 82. Chen VB, Arendall WB, 3rd, Headd JJ, Keedy DA, Immormino RM, Kapral GJ,
788 Murray LW, Richardson JS, Richardson DC. 2010. MolProbity: all-atom structure
789 validation for macromolecular crystallography. *Acta Crystallogr D Biol Crystallogr*
790 66:12-21.
- 791 83. Krissinel E, Henrick K. 2004. Secondary-structure matching (SSM), a new tool for
792 fast protein structure alignment in three dimensions. *Acta Crystallogr D Biol*
793 *Crystallogr* 60:2256-68.
- 794

Mobile loop tunes reaction mechanism of metallo- β -lactamases

795

796

797 **TABLES**

798 **Table 1.** Antimicrobial susceptibility profiles of *E. coli* DH5 α pMBLe producing NDM-1 and
799 its variants at loop L3. Minimum Inhibitory Concentrations (mg/L).

Variant	Imipenem	Meropenem	Piperacillin	Cefotaxime	Ceftazidime	Cefepime
NDM-1	4	2	128	64	1024	16
L3IMP	2	1	64	16	256	16
L3VIM	1	1	64	32	256	2
L3Pro	1	1	16	64	256	0.5
DH5 α pMBLe	0.25	0.03	2	0.03	0.25	0.016

800

801

802 **Table 2.** Melting temperatures (T_M) of apo- and holo-enzymes measured by thermal shift
803 assay.

804

Variant		T_M ($^{\circ}\text{C}$)	ΔT_M ($^{\circ}\text{C}$)
NDM-1	Holo	56.6 ± 0.1	18.3 ± 0.1
	Apo	38.3 ± 0.1	
L3IMP	Holo	55.3 ± 0.1	24.4 ± 0.4
	Apo	30.9 ± 0.3	
L3VIM	Holo	55.2 ± 0.1	31.5 ± 0.1
	Apo	23.7 ± 0.1	
L3Pro	Holo	52.5 ± 0.1	19.0 ± 0.2
	Apo	33.5 ± 0.1	

805
806

807 **Table 3.** Steady-state kinetic parameters for the NDM-1 and its L3 variants. Experimental
 808 conditions: buffer 10 mM HEPES pH 7.5, 200 mM NaCl, 20 μ M ZnSO₄, 20 μ g/mL bovine
 809 serum albumin (BSA); 30 °C. ND, not determined.

Substrate	Variant	K_M (μ M)	k_{cat} (s^{-1})	k_{cat}/K_M (μ M ⁻¹ s^{-1})
Imipenem	NDM-1	150 \pm 30	570 \pm 30	4 \pm 1
	L3IMP	60 \pm 10	160 \pm 6	2.7 \pm 0.5
	L3VIM	136 \pm 7	631 \pm 9	4.6 \pm 0.3
	L3Pro	780 \pm 90	1200 \pm 60	1.5 \pm 0.2
Meropenem	NDM-1	140 \pm 20	960 \pm 40	7 \pm 1
	L3IMP	90 \pm 10	39 \pm 1	0.4 \pm 0.1
	L3VIM	540 \pm 50	1810 \pm 70	3.4 \pm 0.4
	L3Pro	1100 \pm 200	2500 \pm 200	2.3 \pm 0.6
Ertapenem	NDM-1	25 \pm 2	420 \pm 10	17 \pm 2
	L3IMP	29 \pm 6	29 \pm 1	1.0 \pm 0.2
	L3VIM	110 \pm 20	750 \pm 40	5 \pm 1
	L3Pro	270 \pm 20	710 \pm 20	2.6 \pm 0.3
Penicillin G	NDM-1	80 \pm 10	690 \pm 20	8 \pm 1
	L3IMP	13 \pm 1	272 \pm 4	21 \pm 2
	L3VIM	40 \pm 5	323 \pm 9	8 \pm 1
	L3Pro	690 \pm 99	755 \pm 49	1.1 \pm 0.1
Piperacillin	NDM-1	120 \pm 10	1190 \pm 40	10 \pm 1
	L3IMP	67 \pm 8	232 \pm 6	3.5 \pm 0.5
	L3VIM	410 \pm 30	1820 \pm 70	4.4 \pm 0.5
	L3Pro	700 \pm 100	630 \pm 70	0.9 \pm 0.2
Ceftazidime	NDM-1	60 \pm 10	620 \pm 20	10 \pm 2
	L3IMP	60 \pm 10	131 \pm 5	2.2 \pm 0.4
	L3VIM	58 \pm 8	250 \pm 8	4.1 \pm 0.7
	L3Pro	90 \pm 20	120 \pm 10	1.3 \pm 0.4
Cefepime	NDM-1	50 \pm 10	300 \pm 20	6 \pm 2
	L3IMP	6.1 \pm 0.6	178 \pm 2	28 \pm 3
	L3VIM	ND	ND	1.2 \pm 0.1
	L3Pro	ND	ND	0.9 \pm 0.5

Mobile loop tunes reaction mechanism of metallo- β -lactamases

Nitrocefin	NDM-1	1.3 ± 0.3	38 ± 2	29 ± 8
	L3IMP	2.9 ± 0.9	67 ± 7	23 ± 3
	L3VIM	4.0 ± 0.9	48 ± 3	12 ± 3
	L3Pro	2.6 ± 0.5	85 ± 4	32 ± 1

810

811 **FIGURE LEGENDS**

812 **Fig. 1.** Engineered substitutions of loop L3 in NDM-1. Sequence alignment of the L3
813 variants, highlighting the differences at the loop L3 region, including the standard BBL
814 numbering (28).

815

816 **Fig. 2.** Expression levels and Zn(II) limitation susceptibility of NDM-1 and the L3 variants.
817 (A) Immunoblot demonstrating steady-state expression in *E. coli* DH5 α . Proteins were
818 detected from whole cell lysates (lanes 2-5 and 14), spheroplasts (lanes 6-9) and
819 periplasmic extracts (lanes 10-13). Wild type NDM-1 (W) corresponds to lane 2, 6 and 10;
820 L3IMP (I) lanes 3, 7 and 11; L3VIM (V) lanes 4, 8 and 12; L3Pro (P) lanes 5, 9 and 13, and
821 empty plasmid (E) lane 14. Lane 1 shows protein ladder marker. GroEL molecular weight is
822 60 kDa and MBP 47 kDa (B) Immunoblot demonstrating steady-state expression of wild
823 type NDM-1 and the L3 variants in *E. coli* DH5 α treated with DPA. After induction, cells
824 were incubated with (+) or without (-) DPA and protein expression was detected from of
825 whole cell lysates. Wild type NDM-1 (W) corresponds to lane 2-3, L3IMP (I) lanes 4-5,
826 L3VIM (V) lanes 6-7, L3Pro (P) lanes 8-9 and empty plasmid (E) lanes 10-11. Untreated
827 cells were loaded before treated ones. Lane 1 shows protein ladder marker. (C)
828 Antimicrobial susceptibility profiles of *E. coli* DH5 α pMBLe producing β -lactamases against
829 cefotaxime at increasing DPA concentrations. *E. coli* DH5 α expressing NDM-1 is shown in
830 blue; L3IMP in green, L3VIM in red; and L3Pro in orange.

831

832 **Fig. 3.** Difference spectrum of Co(II)-substituted wild type NDM-1 and of the L3 variants.
833 The difference spectrum of the Co(II)-substituted M β LS were obtained by subtraction of the

834 spectrum of the non-metallated β -lactamase from the one corresponding to the final bi-
835 Co(II) substituted variant. The difference spectrum of the wild type NDM-1 is shown in blue;
836 L3IMP in green, L3VIM in red and L3Pro in orange.

837

838 **Fig. 4.** X-ray crystal structures of the L3IMP and L3Pro variants compared to NDM-1.
839 Crystal structures of NDM-1 (PDB code: 3SPU, chain D) in blue, L3IMP in green (PDB
840 code: 6C6I, 1.65 Å) and L3Pro in orange (PDB code: 6CAC, 1.80 Å). The images were
841 generated after the complete alignment of NDM-1 and the two L3 variants. (A) The loop L3
842 position is highlighted in a darker color. (B) Relevant conserved amino acids from the active
843 sites of NDM-1 (blue), L3IMP (green), and L3Pro (orange) are represented by sticks; metal
844 ions (Zn(II) in grey and Cd(II) in light orange) and water molecules (red) are represented as
845 spheres. The position and orientation of the metal ligands is conserved among the three
846 structures. The distances between the ions in the two sites are very similar (≈ 3.8 Å) among
847 the different proteins. The position of the ions in the DCH site displays a slight variability
848 among the structures while in the 3H site the position is unchanged. (C) Angle determined
849 by the loop L3 and the plane of the active site of each mutant. The angles were calculated
850 between the Zn1, C α of Ser69 and C α of Gly63. The values obtained for each loop L3 were:
851 L3IMP = 68°, NDM-1 = 88°, and L3Pro = 110°.

852

853 **Fig. 5.** Photodiode array stopped-flow spectra and traces of nitrocefin hydrolysis by NDM-1
854 and its L3 variants. (A) Reaction mechanism for nitrocefin hydrolysis by NDM-1, adapted
855 from Yang et al (32). (B) Electronic absorption spectra upon the reaction of 10 μ M nitrocefin
856 and 10 μ M enzyme in 100 mM HEPES, pH 7.5, 0.2 M NaCl and 0.3 mM ZnSO₄, at 6 °C.
857 The reaction progresses from black to color: NDM-1 in blue, L3VIM in red, L3IMP in green

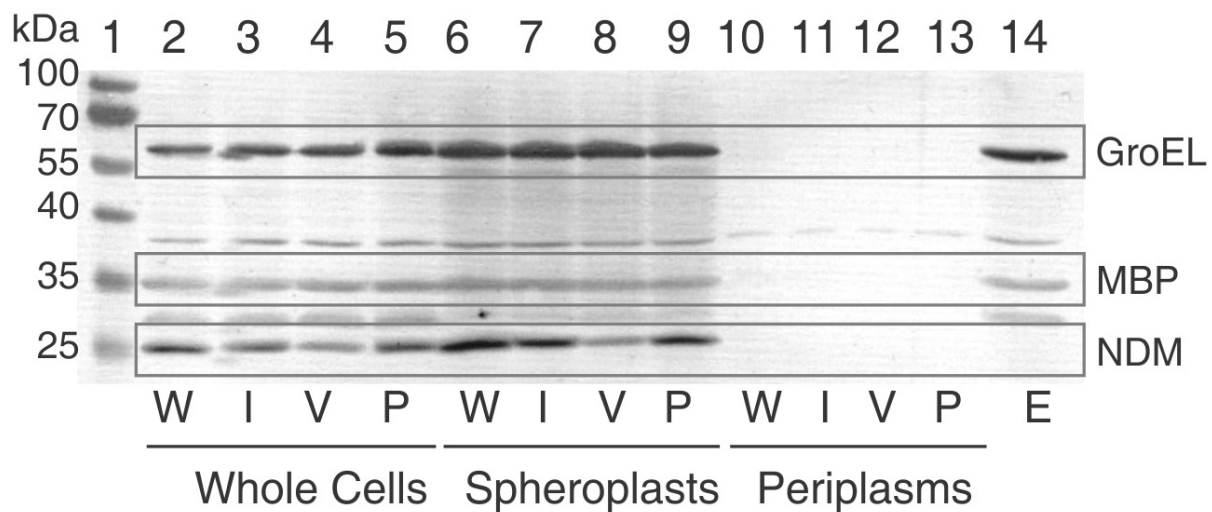
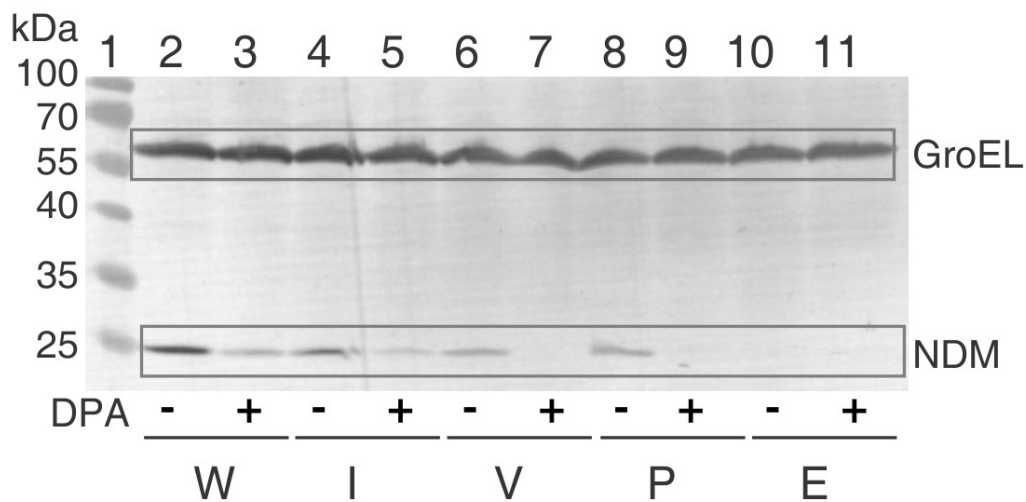
858 and L3Pro in orange. Absorption bands with peaks at 390, 485 and 605 nm correspond to
859 maximum absorption of the substrate, product, and the anionic intermediate of the reaction,
860 respectively. (C) Temporary profiles of substrate (390 nm), intermediate (665 nm) and
861 product (485 nm) during the reaction described in (A). Traces from NDM-1 are shown in
862 blue; L3VIM in red; L3IMP in green and L3Pro in yellow.

863

864 **Fig. 6.** Photodiode array stopped-flow spectra of carbapenems hydrolysis by NDM-1 and
865 the L3 variants. (A) General reaction mechanism for carbapenems hydrolysis by M β Ls,
866 adapted from Lisa, Palacios et al. (33). The ES complex does not accumulate and is hence
867 depicted in a lighter color (grey). (B) Sequence of difference spectra collected upon the
868 reaction of 100 μ M imipenem and 100 μ M β -lactamase. The reactions progress from black
869 to color: NDM-1 blue, L3VIM red, L3IMP green and L3Pro orange. The ionic intermediates,
870 EI1 and EI2, were detected as absorption bands with maximum at 390 and 343 nm. The
871 time interval spans up to 0.2 s. (C) Sequence of difference spectra upon the reaction of 100
872 μ M meropenem and 100 μ M enzyme. The reactions progresses from black to color: NDM-1
873 in blue, L3VIM in red, L3IMP in green and L3Pro in orange. The ionic intermediates, EI1
874 and EI2, are detected as absorption bands with maximum at 390 and 330 nm. The time
875 interval spans up 0.2 s.

BBL	53	54	55	56	57	58	59	60	61	62	63	64	65	66	67	68	69	70	71	
NDM-1	W	Q	H	T	S	Y	L	D	M	P	G	F	G	A	V	A	-	S	N	G
L3IMP	W	Q	H	T	S	F	E	E	V	N	G	W	G	V	V	P	-	S	N	G
L3VIM	W	Q	H	T	A	T	Q	S	F	D	G	-	A	V	Y	P	-	S	N	G
L3Pro	W	Q	H	T	S	Y	L	D	M	P	G	F	G	A	V	A	P	S	N	G

Loop L3

A**B****C**